ORIGINAL ARTICLE

Silencing circPalm2 inhibits sepsis-induced acute lung injury by sponging miR-376b-3p and targeting MAP3K1

Pengfei Gao[1,2] · Wenying Duan[1] · Huiyan Shi[4] · Qingxiu Wang[1,3]

Abstract

The apoptosis and inflammation of pulmonary epithelial cells are important pathogenic factors of sepsis-induced acute lung injury (ALI). Upregulation of circPalm2 (circ_0001212) expression levels has been previously detected in the lung tissue of ALI rats. Herein, the biological significance and detailed mechanism of circPalm2 in ALI pathogenesis were investigated. In vivo models of sepsis-induced ALI were established by treating C57BL/6 mice with cecal ligation and puncture (CLP) surgery. Murine pulmonary epithelial cells (MLE-12 cells) were stimulated with lipopolysaccharide (LPS) to establish in vitro septic ALI models. MLE-12 cell viability and apoptosis were evaluated by CCK-8 assay and flow cytometry analysis, respectively. The pathological alterations of the lung tissue were analysed based on hematoxylin-eosin (H&E) staining. Cell apoptosis in the lung tissue samples was examined by TUNEL staining assay. LPS administration suppressed the viability and accelerated the inflammation and apoptotic behaviours of MLE-12 cells. CircPalm2 displayed high expression in LPS-stimulated MLE-12 cells and possessed circular characteristics. The silencing of circPalm2 impeded apoptosis and inflammation in LPS-stimulated MLE-12 cells. Mechanistically, circPalm2 bound with miR-376b-3p, which targeted MAP3K1. In rescue assays, MAP3K1 enhancement reversed the repressive effects of circPalm2 depletion on LPS-triggered inflammatory injury and MLE-12 cell apoptosis. Furthermore, the lung tissue collected from CLP model mice displayed low miR-376b-3p expression and high levels of circPalm2 and MAP3K1. CircPalm2 positively regulated MAP3K1 expression by downregulating miR-376b-3p in murine lung tissues. Importantly, circPalm2 knockdown attenuated CLP-induced inflammation, apoptosis, and pathological alterations in lung tissues collected from mice. Silenced circPalm2 inhibits LPS-induced pulmonary epithelial cell dysfunction and mitigates abnormalities in lung tissues collected from CLP-stimulated mice via the miR-376b-3p/MAP3K1 axis in septic ALI.

Keywords circPalm2 · miR-376b-3p · MAP3K1 · Acute lung injury · Sepsis · Inflammation

Introduction

Sepsis is a noteworthy cause of high mortality worldwide and can be induced by fungi, viruses or pathogenic bacteria [1]. Severe sepsis can lead to multiorgan dysfunction and even the death of patients [2]. Acute lung injury (ALI) is a severe syndrome that includes multiple acute respiratory failure diseases, and its incidence is clinically associated with sepsis [3]. Currently, there are no recommended standard therapies for sepsis-induced ALI, and finding ways to prevent and treat ALI has become urgent [4, 5]. Due to the complex pathogenesis of septic ALI, it is of great significance to identify reliable biomarkers and potential molecular regulatory mechanisms associated with the initiation and progression of this disease.

✉ Qingxiu Wang
qxw1123@yeah.net

1 Shanghai East Clinical Medical College, Nanjing Medical University, No. 150, Jimo Road, Pudong New Area, Shanghai 200120, China

2 Department of Anesthesiology, The Affiliated Huaian No. 1 People's Hospital of Nanjing Medical University, Huaian, Jiangsu 223300, China

3 Shanghai East Hopital, Tongji University School of Medicine, Shanghai 200120, China

4 Jinzhou Medical University, Jinzhou, Liaoning 121001, China

During the pathological processes of septic ALI, the activation of apoptotic and inflammatory pathways results in the aggravation of lung edema, increased pulmonary epithelial permeability and the apoptosis of alveolar epithelial cells [6, 7]. Recent studies have revealed that an increase in proapoptotic proteins in ALI contributes to the apoptotic behaviours of the alveolar epithelium as well as epithelial damage [8]. Persistent elevation of proinflammatory cytokine production is a predictor of death in ALI patients, as multiple reports have demonstrated [9, 10]. These findings indicate that modulation of the inflammatory and apoptotic pathways may be a new strategy to prevent septic ALI pathogenesis.

Circular RNAs (circRNAs) are a group of ubiquitous RNA transcripts with high stability (with no 5′ ends or 3′ tails) [11]. CircRNAs often display tissue-specific or cell-specific expression patterns [12]. Over the past decades, numerous circRNAs have been proven to play important roles in the occurrence of many diseases, such as atherosclerosis, sepsis, and cardiovascular disease [13–15]. In addition, circRNAs also participate in a variety of biological activities, including cell growth, metastasis, invasion, oxidative stress, and the inflammatory response [16].

Emerging evidence has confirmed the promising role of circRNA in the diagnosis or treatment of sepsis-associated ALI [17]. For example, Yang et al. showed that silencing circ0054633 promotes the apoptosis and inflammation of microvascular endothelial cells in ALI induced by sepsis by inhibiting NF-κB signaling [18]. A study reported that 12 upregulated circRNAs and 126 downregulated circRNAs were detected in macrophages extracted from lung tissue of an ALI mouse model of sepsis, suggesting that these circRNAs may be related to the differentiation and polarization of macrophages [19]. CircTMOD3 is highly expressed in lipopolysaccharide (LPS)-stimulated lung fibroblasts, while knockdown of circTMOD3 reduces LPS-induced injury and the inflammatory response in lung fibroblasts [20]. All of these studies indicate that circRNAs exert important functions in the pathology of septic ALI.

CircPalm2 (circ_0001212) is a novel circRNA derived from Palm2. According to a previous study, lung tissues of mice with sepsis exhibit high circPalm2 levels, and P2×7R antagonists exert a protective role in septic ALI pathogenesis by inhibiting circPalm2 [21]. However, the related functions and mechanisms of circPalm2 in sepsis-induced ALI need further exploration.

There are many different regulatory mechanisms of circRNAs in the development of diseases [22]. The most studied regulatory mechanism is the competing endogenous RNA (ceRNA) network, in which circRNAs sponge microRNAs (miRNAs) to regulate the expression levels of miRNA downstream genes [23]. MiRNAs, small noncoding RNAs with 20–24 nucleotides, account for approximately 1% of the human genome but regulate as much as 50% of

all human protein-coding genes [24]. Accumulating studies have revealed the ceRNA network mediated by circRNAs in septic ALI. For example, Jiang et al. demonstrated that circC3P1 attenuates pulmonary injury and inflammation in sepsis-induced ALI by targeting miR-21, indicating that circC3P1 is a potential biomarker for this disease [25]. CircN4 bp1 serves as a competing endogenous RNA (ceRNA) against miR-138-5p to modulate EZH2 expression, thereby decreasing survival time and facilitating the activation of M1 macrophages in mice with septic ALI [26]. CircANKRD36 aggravates septic ALI pathogenesis by elevating LPS-stimulated RAW264.7 cell migration and viability by modulating the miR-330/ROCK1 axis [27].

Herein, we hypothesized that circPalm2 functions as a ceRNA to participate in septic ALI development. To test our hypothesis, we established in vivo septic ALI models using C57BL/6 mice with cecal ligation and puncture (CLP) treatment and in vitro septic ALI models using LPS-stimulated murine pulmonary epithelial cells (MLE-12 cells). Subsequently, the specific mechanism underlying circPalm2 and its impact on MLE-12 cell dysfunction after LPS exposure as well as on lung injury in mice subjected to CLP surgery were evaluated. This work might have revealed novel diagnostic and therapeutic targets for septic ALI.

Materials and methods

Cell treatment

MLE-12 cells (ATCC, Manassas, VA, USA) were cultured in DMEM (Gibco, Guangzhou, China) containing 5% fetal bovine serum (Gibco) and 1% penicillin/streptomycin solution (Gibco) at 37 °C with 5% CO_2. To induce septic ALI in vitro, MLE-12 cells were administered 50 μg/ml LPS for 16 h [28]. To inhibit JNK1/2 signalling, MLE-12 cells were pretreated with 40 μM JNK-in-8 (MedChem Express, Monmouth Junction, NJ, USA) for 1 h [29]. Untreated MLE-12 cells served as the control (Con) group.

Animal model and grouping

Sixty adult male C57BL/6 mice were donated by Professor Lu Ying. All animals were raised in a specific pathogen-free (SPF) environment at the Experimental Animal Center of Tongji University and received water and food *ad libitum*. The animal experiments in this study were performed in accordance with the Guide for Care and Use of Laboratory Animals approved by the Animal Research Committee of the Hospital. Adenoviral vectors containing sh-circPalm2 (Ad-Sh-circPalm2) and its negative control (Ad-NC) were purchased from Genechem (Shanghai, China).

The grouping of mice was as follows: sham group, CLP group, CLP + Ad-NC group and CLP + Ad-Sh-circPalm2 group, with 15 mice per group. To establish the CLP-ALI murine model, mice in the last three groups were first anaesthetized with 50 mg/kg pentobarbital sodium (1%, Sigma−Aldrich, St. Louis, MO, USA). Next, a 2 cm midline incision was made in the lower abdomen, and a 5-0 suture was used to ligate the exposed cecum at the 1 cm distal tip. A 21 G needle was used to puncture the ligated cecum and overflow the intestinal contents. Afterwards, the cecum was returned to its normal position, and the abdominal cavity was closed. The CLP surgery was performed following a previous description [30, 31]. For sham-operated mice, a lower-midline incision was made, and no manipulation of the cecum was performed.

The delivery of adenoviral vectors was conducted as previously described [25, 32]. One week before CLP treatment, the CLP + Ad-Sh-circPalm2 group was intravenously injected with 20 μL of Ad-Sh-circPalm2 (10^7 particles/μL) via the tail vein, and the CLP + Ad-NC group received an equivalent amount of Ad-NC in the same way.

The body weight of each group was recorded once each day for 9 consecutive days after CLP surgery using an electronic scale (Hirp Trading Co., Ltd., Shanghai, China). At the end of this experiment, mice from each group were euthanized by CO_2 inhalation. After that, the lungs of the mice were harvested and stored in a -80 °C freezer until use. One part of the lung tissues was utilized for extracting RNAs and proteins. Another part of the lung tissues was fixed with 10% formalin for further pathological analysis.

Hematoxylin-eosin (H&E) staining

The fixed portion of the murine lung tissue samples were embedded in paraffin, cut into slices (5 μm thickness), dewaxed using xylene and rehydrated in gradient ethanol. Afterwards, the slices were stained with hematoxylin for 15 min and eosin (Sigma−Aldrich) for 10 min. After staining, the lung tissues were observed under a light microscope (Olympus, Tokyo, Japan). In each sample, five randomly selected fields were scored, and the lung injury degree was determined according to the previous lung injury scoring criterion [33].

Enzyme-linked immunosorbent assay (ELISA)

The accumulation of inflammatory factors in MLE-12 cell lysates and lung tissue homogenates was analysed utilizing corresponding ELISA kits, including a TNF-α ELISA kit (SND-R635, Chuzhou Shinoda Biological Technology Co., Ltd., China), an IL-1β ELISA kit (SND-R418, Shinoda), and an IL-6 ELISA kit (SND-R734, Shinoda). A microplate reader (Power Wave; Bio-Tek, Biotek Winooski, VT, USA) was utilized to detect the absorbance at a wavelength of 450 nm.

RT−qPCR

RNA extraction from lung tissue and MLE-12 cells was performed with TRIzol reagent (Life Technologies, USA). The extracted RNA was reverse transcribed into cDNA utilizing ReverTra Ace qPCR RT kits (Toyobo, Japan) as instructed by the supplier. Next, in accordance with the manufacturer's directions, quantitative PCR was carried out utilizing the SYBR Premix Ex TaqTM II reagent kit (RR820A, Takara) on a real-time qPCR system (ABI, 7500, ABI Company, Oyster Bay, NY, USA). Calculated by the $2^{-\Delta\Delta Ct}$ method [34], circPalm2 and mRNA expression levels were normalized to GAPDH, and miRNA expression was normalized to U6. The sequences of the primers are presented in Table 1.

Treatment with actinomycin D and RNase R

For actinomycin D (ActD) treatment, MLE-12 cells were exposed to 2 μg/ml ActD (Sigma−Aldrich) and harvested at the indicated time points (0 h, 4 h, 8 h, 12 h, and 24 h). For RNase R treatment, 2 μg of total RNA was incubated with 3 U/μg of RNase R (Sigma−Aldrich) at 37 °C for 20 min and

Table 1 Primer sequences for RT-qPCR.

Gene	Sequence (5′-3′)
circPalm2 forward	CCCCAGCTATATACGCCATG
circPalm2 reverse	GTTTTCTACCACGGTGCCTC
miR-330-5p forward	TCTCTGGGCCTGTGTCTTAGGC
miR-330-5p reverse	CAGTGCGTGTCGTGGAGT
MAP3K1 forward	CATGCAAGATGGCCATCAC
MAP3K1 reverse	GAAGAATTGCCCAGCATCC
Scd2 forward	CCACAGAACATACAAGGCA
Scd2 reverse	TACACGTCATTCTGGAACG
Hnrnpa0 forward	GAGATCATTGCCGACAAGC
Hnrnpa0 reverse	TCTGGAAGTAGACGAAGCC
miR-326-3p forward	CCTCTGGGCCCTTCCTCCAGTGT
miR-326-3p reverse	GTGCAGGGTCCGAGGT
miR-7661-3p forward	ACACTCCAGCTGGGTTGACTCCCAGTTTCTCTCTGC
miR-7661-3p reverse	CTCAACTGGTGTCGTGGA
miR-376b-3p forward	GCCGAGATCATAGAGGAAAATC
miR-376b-3p reverse	CTCAACTGGTGTCGTGGA
miR-3077-3p forward	GGAATGAACGCCATCAACC
miR-3077-3p reverse	CTCATTCTCCTCCAGCAGAG
Gapdh forward	AGGTCGGTGTGAACGGATTTG
Gapdh reverse	GGGGTCGTTGATGGCAACA
U6 forward	ACCC TGAGAAATACCCTCACAT
U6 reverse	GACGACTGAGC CCCTGATG

70 °C for 5 min. The levels of linear Palm2 and circPalm2 were estimated using RT−qPCR analysis.

Nuclear-cytoplasmic fractionation assay

After MLE-12 cells were centrifuged at 4 °C for 5 min, cytoplasmic RNA was extracted from the supernatant, while the precipitates were collected for nuclear RNA extraction. The PARIS™ Kit (Thermo Fisher Scientific) was utilized for RNA extraction. The percentages of circPalm2, GAPDH (cytoplasmic control) and U6 (nuclear control) in the two fractions were determined by RT−qPCR analysis.

Transfection of plasmids into MLE-12 cells

The plasmids were provided by GenePharma (Shanghai, China). Short hairpin RNA (shRNA) against circPalm2 (sh-circPalm2; sequence: GCATCAGCTTACAGTTCAA, TTG AACTGTAAGCTGATGC) was used to knockdown circPalm2 with sh-NC (sequence: CTCAGTCTAGTTGCAAAA C, GTTTTGCAACTAGACTGAG) as a negative control. The miR-376b-3p mimics (sequence: UUCACCUACAAG GAGAUACUA) were used to overexpress miR-376b-3p with NC mimic (sequence: CGCGCGGGUGUAUGUCUU UCCU) as the control. The MAP3K1 sequence was inserted into the pcDNA3.1 vector to overexpress MAP3K1, and the empty vector was used as the control. When the cell confluence reached 80%, MLE-12 cells were transfected with 10 nM pcDNA3.1/MAP3K1, 50 nM sh-circPalm2, 40 nM miR-376b-3p mimics or 50 nM of their corresponding negative controls using Lipofectamine 2000 (Invitrogen, CA, USA) at 37 °C for 48 h based on the supplier's guidance. The efficacy of plasmid transfection was measured by RT-qPCR.

Western blotting

Protein extraction from tissue and cells was conducted using RIPA lysis buffer (PH0316, PHYGENE, Fuzhou, China). A BCA protein quantitative kit (E112-01/02, Vazyme, Nanjing, China) was employed for the quantification of total proteins. Denaturation was achieved by boiling the protein samples for 5 min following concentration adjustment. The supernatant liquid was added to 2 × SDS−PAGE loading buffer. After being mixed well and heated at 95 °C, the protein contents were subjected to SDS-PAGE and then transferred to PVDF membranes. The membranes were blocked with TBST solution supplemented with 3% BSA for 1 h followed by incubation with the diluted primary antibodies anti-Bax (ab32503, 1/2000), anti-Bcl-2 (ab182858, 1/2000), anti-MAP3K1 (ab220416, concentration: 1 μg/ml), and anti-GAPDH (ab181603, 1/10,000) at 4 °C with slow shaking overnight. The membranes were then incubated with the diluted secondary antibody (ab102248, 1/1000) after being rinsed with TBST five times. Abcam (Cambridge, MA, USA) provided all of the antibodies used in our study. An ECL detection kit (Bio-Rad, Hercules, CA, USA) was used for visualization of the blot, and the intensity was analysed using Image Lab software (Bio-Rad).

Cell counting kit-8 (CKK-8) assay

After the indicated transfection, the cells were plated into 96-well plates (3×10^4 cells/well). Then, 10 μL Cell Counting Kit-8 (CCK-8) solution (Dojindo, Tokyo, Japan) was added to the plates, followed by incubation for another four hours at room temperature. A microplate reader (BMG Labtech, Germany) was used to measure the optical density (OD) values at a wavelength of 450 nm.

Flow cytometry analyses

For cell cycle analysis, MLE-12 cells were centrifuged at $800 \times g$ for 6 min and then stained with a total of 1 ml propidium iodide (PI; 20 mg/ml) and RNase (10 U/ml) at 37 °C for 30 min. Finally, FACScan flow cytometry (BD Biosciences, San Jose, CA, USA) was applied to analyse cell cycle progression.

For cell apoptosis detection, the Annexin V-FITC Apoptosis Detection Kit (Abcam) was used. In brief, MLE-12 cells with different treatments were collected and incubated with Annexin V-FITC solutions (1 ml) and PI solution (5 μl) for 15 min in the dark. Then, the binding buffer (400 μl) was added to the cells. Finally, flow cytometry (FACScan; BD Biosciences) was employed for MLE-12 cell apoptosis detection.

Luciferase reporter assay

The possible binding sites between circPalm2 and miR-376b-3p were sought using the bioinformatics tool starBase [35], and a binding site for miR-376b-3p in the MAP3K1 3'UTR was predicted with the tool TargetScan [36]. The wild-type (Wt) or mutated (Mut) specific sequence of circPalm2 or the MAP3K1 3' untranslated region (UTR) was cloned into pmirGLO vectors (E1330, Promega, USA) to establish the circPalm2-Wt/Mut reporters or MAP3K1 3'UTR-Wt/Mut reporters. MiR-376b-3p mimics or NC mimics were cotransfected with pmirGLO-circPalm2-Wt/Mut or pmirGLO-MAP3K1 3'UTR-Wt/Mut into MLE-12 cells using Lipofectamine 2000 (Invitrogen). After 48 h of cotransfection, the luciferase activity levels were tested with the Luciferase Reporter Assay System (Promega). The relative firefly luciferase activity was normalized to Renilla luciferase activity.

Statistical analysis

Experimental data were analysed with SPSS 18.0 software (SPSS Inc., Chicago, IL, USA) and are presented as the mean ± standard deviation. Difference comparisons between two groups were evaluated using Student's t test, and those among more groups were analysed using one-way analysis of variance (ANOVA) and the Holm−Sidak post hoc test. Gene expression correlation in lung tissue was confirmed using Pearson correlation analysis. $p < 0.05$ was considered statistically significant.

Results

LPS induces MLE-12 cell apoptosis, cell cycle arrest, and the inflammatory response

Initially, MLE-12 cells were stimulated with LPS to establish in vitro models of septic ALI. After LPS stimulation, MLE-12 cell viability was decreased compared with that of the control (Con) group, as revealed by the CCK-8 assay (Fig. 1A). Based on the ELISA results, LPS exposure contributed to the increased accumulation of proinflammatory cytokines (TNF-α, IL-6 and IL-1β) in MLE-12 cells (Fig. 1B), suggesting that LPS treatment triggered an inflammatory response in cells. Flow cytometry analysis showed that LPS increased the proportion of cells in the G1 phase and reduced the proportion of cells in the S phase, which demonstrated that the G1-S cell cycle transition was suppressed by LPS treatment (Fig. 1C). Additionally, LPS stimulation increased the apoptotic rate of MLE-12 cells (Fig. 1D). Furthermore, western blotting validated that LPS-stimulated MLE-12 cells displayed a decline in the anti-apoptotic indicator Bcl-2 protein and an increase in Bax (a pro-apoptotic indicator) protein (Fig. 1E) compared to the untreated cells. Thus, we concluded that LPS induces MLE-12 cell injury by blocking cell cycle progression while accelerating apoptosis and inflammation.
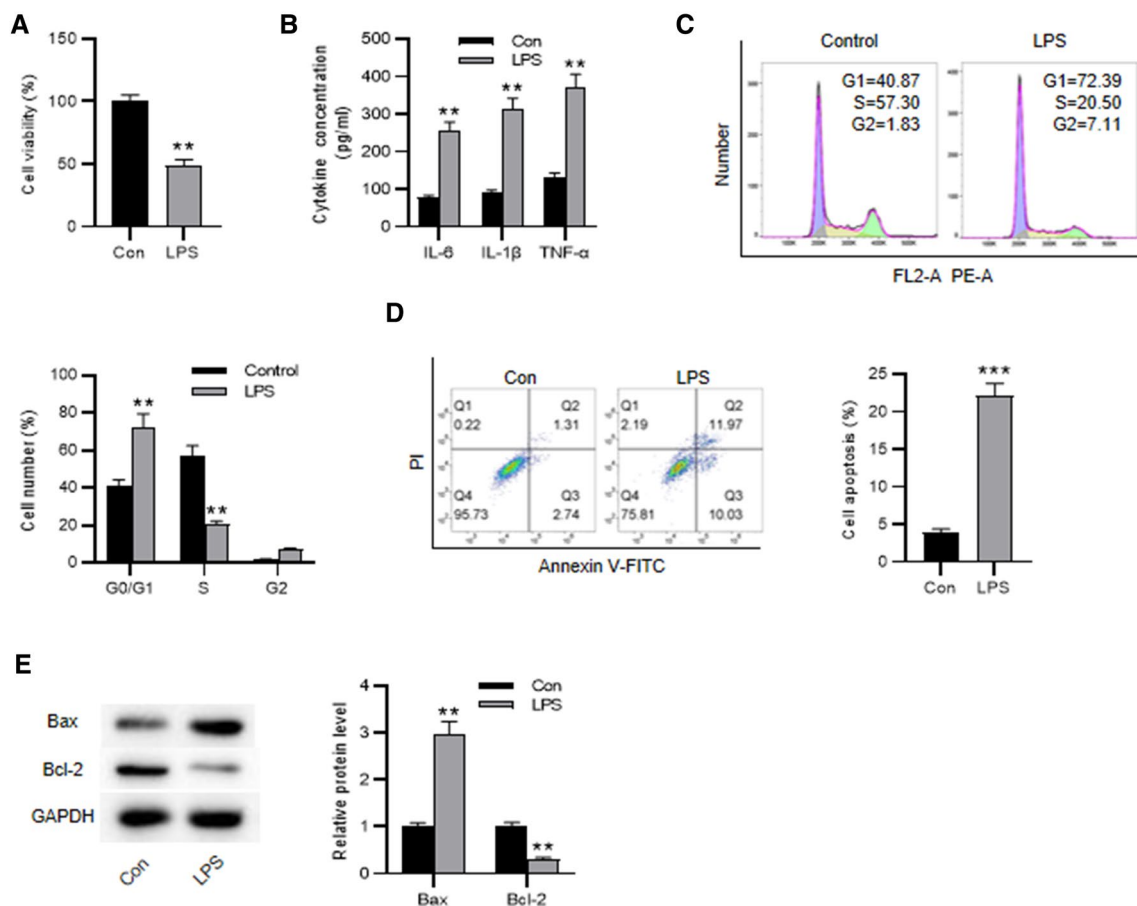
Fig. 1 LPS induces MLE-12 cell apoptosis and inflammation. (**A**) CCK-8 assay for evaluating MLE-12 cell viability in the Con and LPS groups. (**B**) ELISA for determining proinflammatory cytokine concentrations in MLE-12 cells in the Con and LPS groups. (**C, D**) Flow cytometry analysis for determining MLE-12 cell cycle transition and cell apoptosis in the Con and LPS groups. (**E**) Western blotting for determining apoptosis-related marker protein levels in MLE-12 cells of the Con and LPS groups. **$p < 0.01$, ***$p < 0.001$

Characterization of circPalm2

CircPalm2 (circ_0001212) is spliced from exons 2–5 of Palm2 pre-mRNA and located on chr4:57,722,322–57,723,015, as shown by the schematic diagram of the circBase database (http://www.circbase.org/) (Fig. 2A). To determine the stability of circPalm2, the RNA extracted from MLE-12 cells was exposed to RNase R. The linear Palm2 level was reduced sharply in response to RNase R treatment, whereas circPalm2 was almost insensitive to RNase R (Fig. 2B). To further identify the circular characteristics of circPalm2, actinomycin D was used to treat MLE-12 cells. A gradual reduction in mRNA levels was observed in the linear Palm2 group, while circPalm2 levels were more stable in response to actinomycin D treatment (Fig. 2C). These results reveal the circular characteristics of circPalm2. In addition, circPalm2 was highly expressed in LPS-intoxicated MLE-12 cells, in contrast to that in the Con group, indicating the possible involvement of circPalm2 in ALI (Fig. 2D). Moreover, circPalm2 mainly existed in the cytoplasm of MLE-12 cells, implying that circPalm2 can exert its functions at the posttranscriptional level (Fig. 2E).
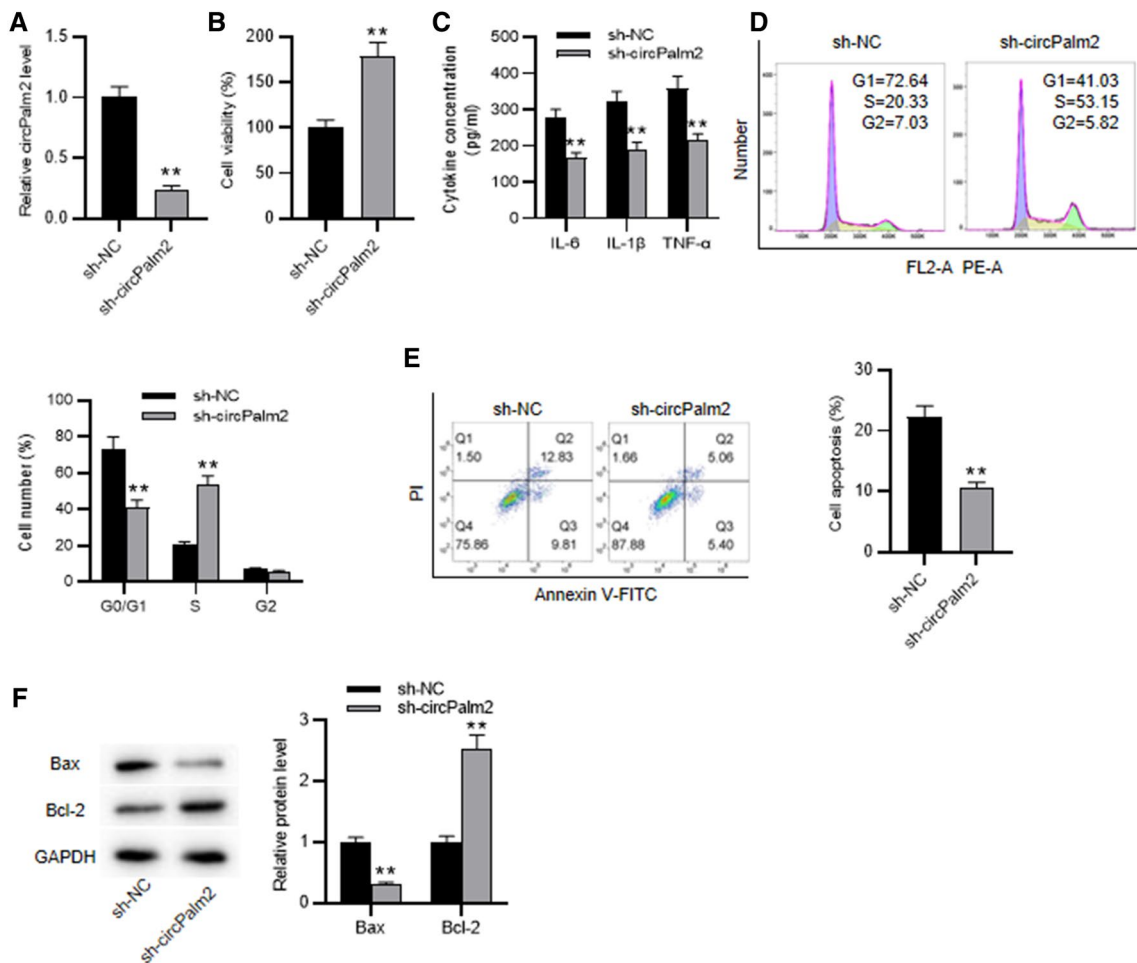
CircPalm2 depletion ameliorates LPS-evoked apoptosis, cell cycle arrest, and inflammation

To determine the biological functions of circPalm2 in ALI pathogenesis, we performed RT−qPCR to measure the knockdown effect of circPalm2 in LPS-stimulated MLE-12 cells. As demonstrated in Fig. 3A, we effectively downregulated circPalm2 levels by transfection with sh-circPalm2. The CCK-8 assay illustrated that silencing circPalm2 led to an increase in the viability of LPS-stimulated MLE-12 cells (Fig. 3B). ELISA indicated that the proinflammatory cytokine concentration in LPS-intoxicated MLE-12 cells was decreased by knockdown of circPalm2 (Fig. 3C). Moreover, silencing of circPalm2 resulted in a reduced proportion of cells in G1 phase and an elevated proportion of cells in S phase relative to the control group (LPS + sh-NC), which implied that cell cycle transition was promoted by circPalm2 silencing (Fig. 3D). In addition, circPalm2 downregulation impeded the apoptotic behaviours of MLE-12 cells stimulated by LPS (Fig. 3E). Silencing of circPalm2 reduced Bax protein levels and increased Bcl-2 protein expression in MLE-12 cells treated with LPS (Fig. 3F). Overall, circPalm2
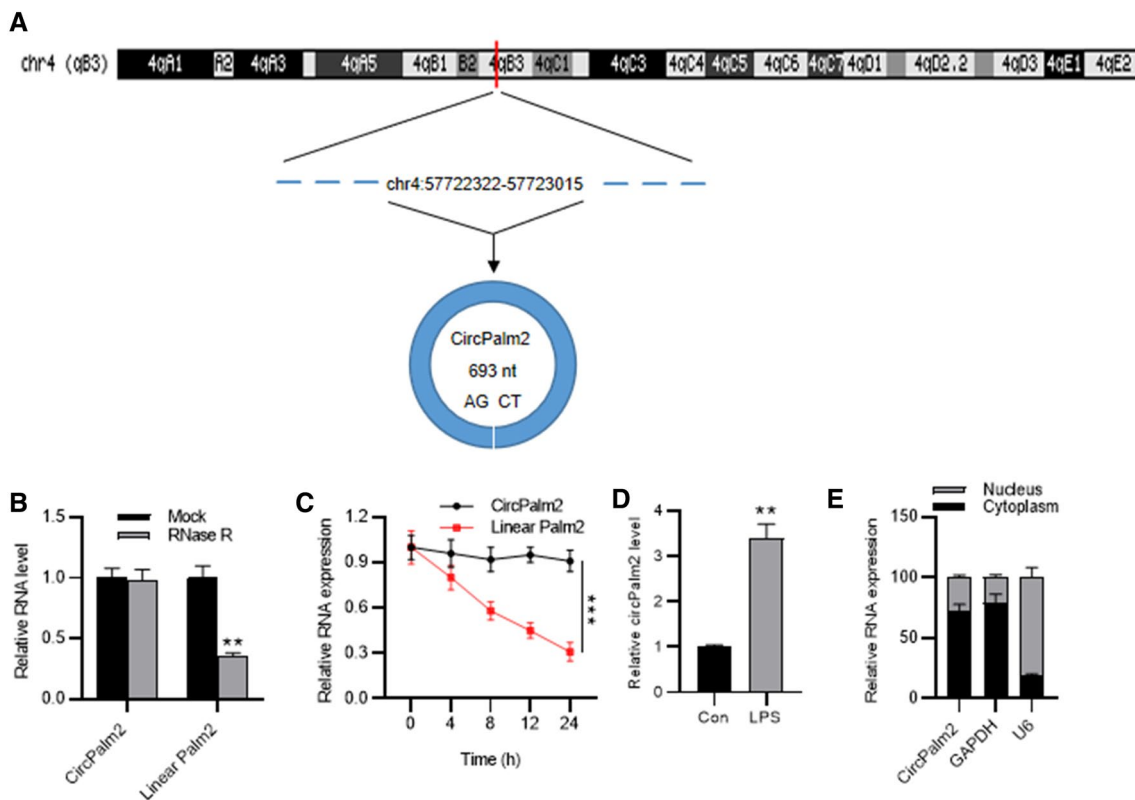
Fig. 2 Characterization of circPalm2. (**A**) Schematic diagram of circPalm2 formed by back-splicing from the Palm2 premRNA at the chromosome, as shown by the circBase database (http://www.circbase.org/). (**B**) The levels of circPalm2 and linear Palm2 were measured after treatment with RNase R. (**C**) CircPalm2 and linear Palm2 levels were estimated after actinomycin D treatment. (**D**) RT−qPCR for evaluating circPalm2 expression in MLE-12 cells of the Con and LPS groups. (**E**) Nuclear-cytoplasmic fractionation assay for determining the subcellular localization of circPalm2 in MLE-12 cells. $**p < 0.01$, $***p < 0.001$

Fig. 3 CircPalm2 depletion ameliorates LPS-evoked MLE-12 cell damage. (**A**) RT−qPCR for transfection efficiency of sh-circPalm2. (**B**) CCK-8 assay for evaluating LPS-treated MLE-12 cell viability after downregulating circPalm2. (**C**) ELISA for determining the proinflammatory cytokine concentration in LPS-stimulated MLE-12 cells after downregulating circPalm2. (**D**, **E**) Flow cytometry analysis for determining LPS-treated MLE-12 cell cycle transition and cell apoptosis after downregulating circPalm2. (**F**) Western blotting for determining apoptosis-related marker protein levels in LPS-stimulated MLE-12 cells after downregulating circPalm2. **$**p < 0.01$

downregulation attenuates LPS-triggered cell apoptosis, cell cycle arrest, and inflammation.

CircPalm2 sponges miR-376b-3p

The circRNA-miRNA−mRNA network was previously reported to be involved in ALI development [37]. To determine the mechanism by which circPalm2 regulates LPS-elicited injury of MLE-12 cells, five potential miRNAs that may interact with circPalm2 were predicted using the tool starBase (Fig. 4A). As denoted in Fig. 4B, LPS treatment decreased miR-376b-3p and miR-330-5p levels in MLE-12 cells. Moreover, qPCR analysis revealed that miR-376b-3p displayed a much higher level in the context of circPalm2 depletion than miR-330-5p (Fig. 4C). Moreover, the interaction between circPalm2 and miR-330-5p has been fully explored [38], and miR-376b-3p was selected for further

investigation. We found that transfection of miR-376b-3p mimics could overexpress miR-376b-3p but did not affect circPalm2 levels in MLE-12 cells (Fig. 4D). A possible binding site between circPalm2 and miR-376b-3p was identified with the tool starBase (Fig. 4E). CircPalm2-Wt relative luciferase activity was markedly reduced by miR-376b-3p overexpression in MLE-12 cells, and circPalm2-Mut activity displayed no significant changes under the same conditions (Fig. 4F). These results indicate that circPalm2 sponges miR-376b-3p in MLE-12 cells.
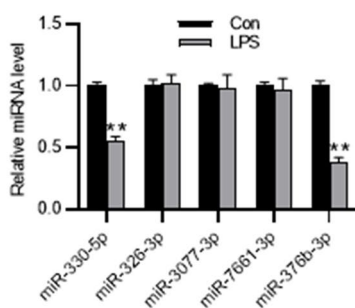
MiR-376b-3p targets MAP3K1

To further investigate the ceRNA network involving circPalm2 in ALI development, 3 potential target mRNAs (*MAP3K1*, *Scd2* and *Hnrnpa0*) possessing binding sites for miR-376b-3p were predicted by the ENCORI website
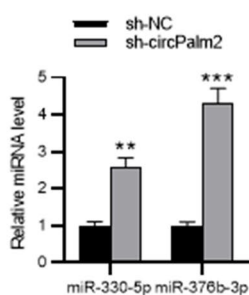
A

B

C

D

E

F
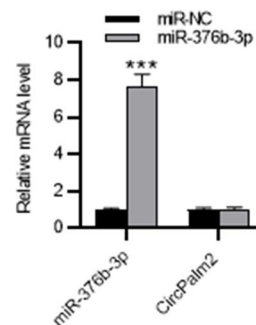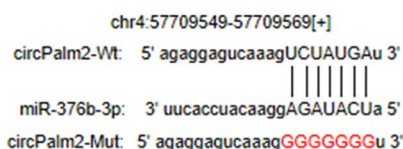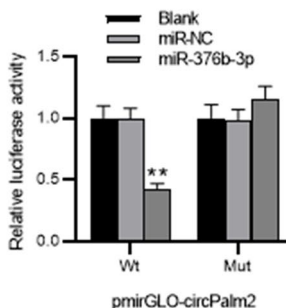

Fig. 4 CircPalm2 sponges miR-376b-3p. (**A**) Potential miRNAs (mmu-miR-330-5p, mmu-miR-326-3p, mmu-miR-3077-3p, mmu-miR-7661-3p and mmu-miR-376b-3p) that can interact with circ-Palm2 were searched on the ENCORI website. (**B**) RT−qPCR for detecting the impact of LPS on miRNAs in MLE-12 cells. (**C**) miR-330-5p and miR-376b-3p expression in response to circPalm2 silencing was measured by qPCR in MLE-12 cells. (**D**) RT−qPCR for

detecting the impact of miR-376b-3p mimics on the levels of miR-376b-3p and circPalm2 in MLE-12 cells. (**E**) Bioinformatics analysis of the possible binding area between circPalm2 and miR-376b-3p. (**F**) Luciferase reporter assays were performed to verify the binding relationship between circPalm2 and miR-376b-3p. *******p* < 0.01, ********p* < 0.001

(condition: AgoExpNum > 6). RT−qPCR analysis revealed that LPS administration only caused upregulation of the *MAP3K1* mRNA level (Fig. 5A). Additionally, treatment with LPS in MLE-12 cells also increased the MAP3K1 protein level (Fig. 5B, C). The binding site between the MAP3K1 3′UTR and miR-376b-3p predicted by ENCORI is presented in Fig. 5D. The results of luciferase

reporter assays verified the suppressive impact of miR-376b-3p upregulation on the luciferase activity level of the MAP3K1-3′UTR-Wt vector, while no obvious change was observed in the MAP3K1-3′UTR-Mut group after overexpressing miR-376b-3p (Fig. 5E). In addition, either miR-376b-3p upregulation or circPalm2 silencing
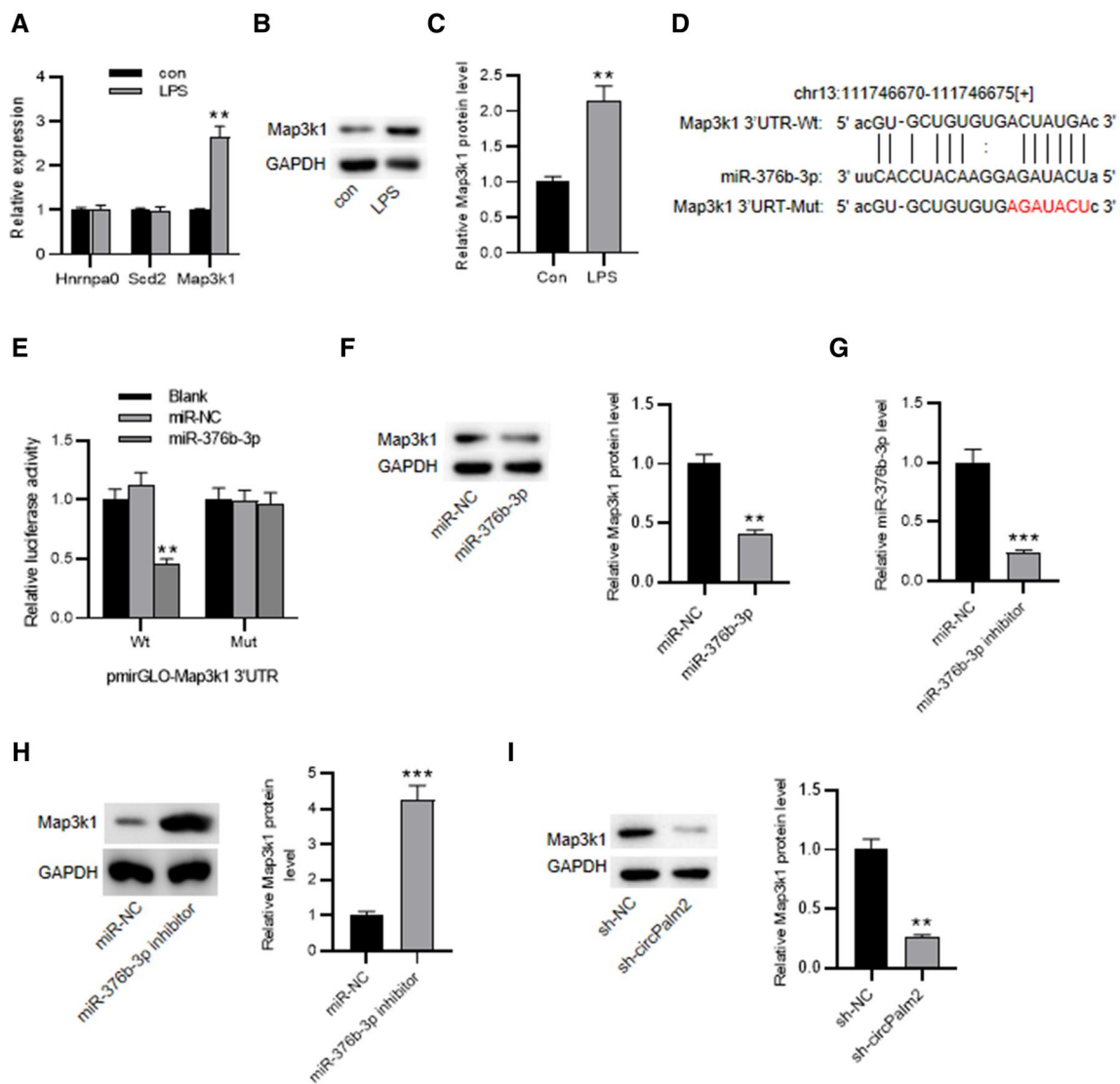
Fig. 5 MiR-376b-3p targets MAP3K1. (**A**) RT−qPCR for detecting the impact of LPS on the mRNA expression of 3 candidate genes (*MAP3K1*, *Scd2* and *Hnrnpa0*) in MLE-12 cells. (**B**, **C**) Western blotting for detecting the impact of LPS on MAP3K1 protein expression in MLE-12 cells. (**D**) According to the prediction from the ENCORI website, a binding site for miR-376b-3p is present in the MAP3K1 3'UTR. (**E**) Luciferase reporter assays were conducted to confirm the interaction between miR-376b-3p and the MAP3K1 3'UTR. (**F**, **H**, **I**) The protein level of MAP3K1 in the context of miR-376b-3p upregulation, miR-376b-3p inhibition, or circPalm2 silencing was measured by western blotting. (**G**) The knockdown efficacy of the miR-376b-3p inhibitor in MLE-12 cells was evaluated by RT−qPCR. **$p < 0.01$, ***$p < 0.001$

decreased the protein level of MAP3K1, as revealed by western blotting (Fig. 5F, I). In contrast, MAP3K1 protein expression was increased in response to miR-376b-3p deficiency (Fig. 5H). The knockdown efficacy of the miR-376b-3p inhibitor (76% decrease) in MLE-12 cells was calculated based on RT−qPCR (Fig. 5G). The above findings indicated that miR-376b-3p targets MAP3K1 and that miR-376b-3p negatively regulates MAP3K1 levels, while circPalm2 positively regulates MAP3K1 expression.

miR-376b-3p overexpression attenuates LPS-induced MLE-12 cell apoptosis, cell cycle arrest, and inflammation by regulating MAP3K1

Subsequently, the influence of miR-376b-3p overexpression on LPS-induced cell injury and inflammation was evaluated, and whether miR-376b-3p affects cell behaviors by regulating MAP3K1 was explored. After transfection with pcDNA3.1/MAP3K1, MAP3K1 mRNA and protein levels were upregulated in LPS-treated MLE-12
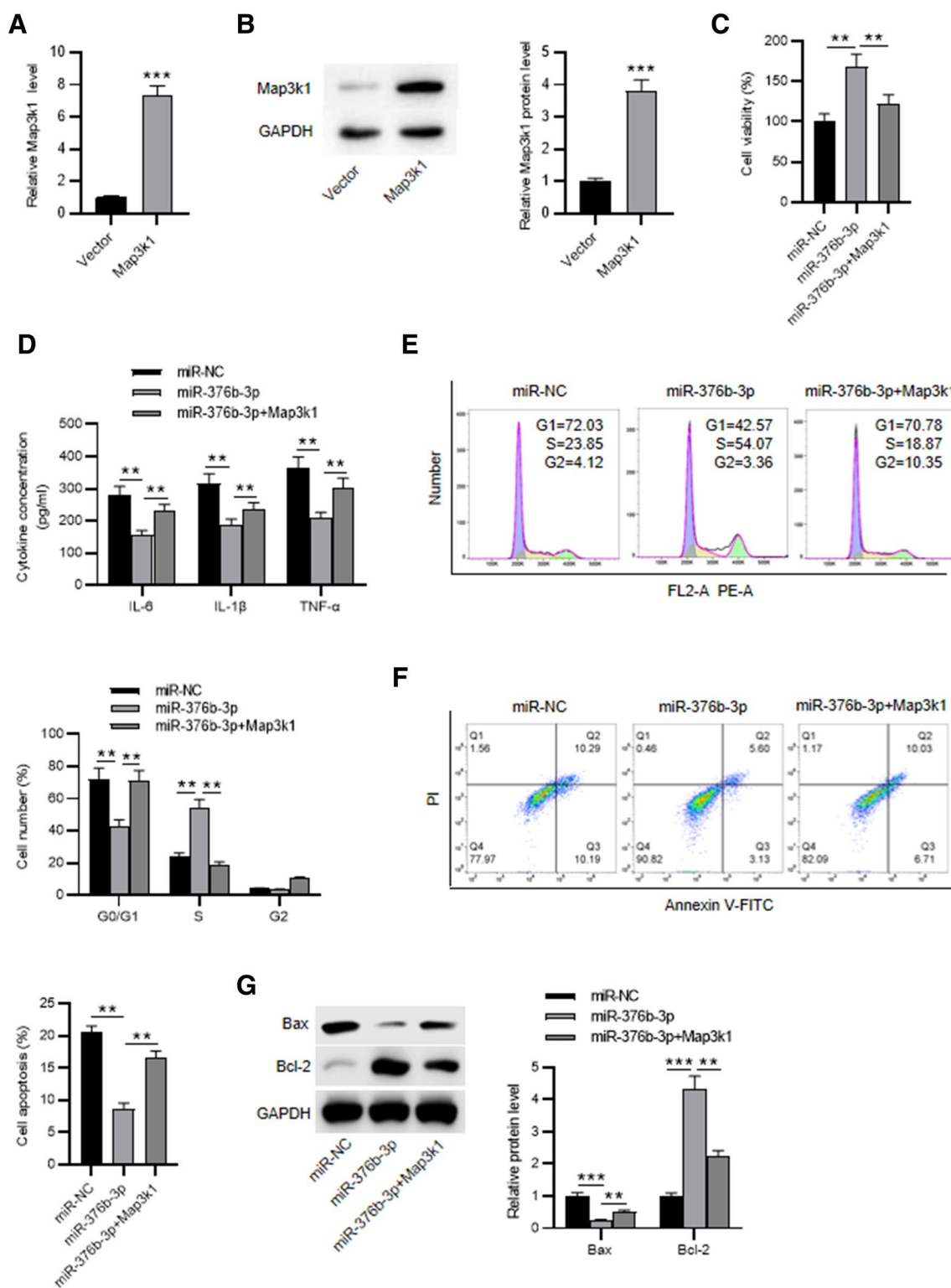
Fig. 6 miR-376b-3p overexpression attenuates LPS-induced cell apoptosis and the inflammatory response, and the alterations were counteracted by overexpression of MAP3K1. (**A**, **B**) RT−qPCR and western blotting for evaluating the transfection efficiency of pcDNA3.1/MAP3K1. (**C**) CCK-8 assay for detecting cell viability after LPS treatment and plasmid (miR-NC, miR-376b-3p mimics, or miR-376b-3p mimics + pcDNA3.1/MAP3K1) transfection. (**D**) ELISA for measuring the concentrations of inflammatory cytokines in cells with the above treatment. (**E**, **F**) Flow cytometry analysis for the detection of cell cycle progression and cell apoptosis. (**G**) Protein levels of apoptosis-related genes were quantified using western blotting. **$p < 0.01$, ***$p < 0.001$

cells (Fig. 6A, B). In comparison to the control group (LPS + miR-NC), the overexpressed miR-376b-3p group showed increased cell viability, and the increase in cell viability induced by miR-376b-3p was offset by overexpression of MAP3K1 (Fig. 6C). According to ELISA, overexpressing miR-376b-3p induced a reduction in inflammatory factors, and the changes were reversed in the context of both miR-376b-3p and MAP3K1 overexpression (Fig. 6D). Moreover, the reduction in the percentage of cells in G1 phase and the increase in the number of cells in S phase suggested a promoting impact of miR-376b-3p on cell cycle transition, and the alteration mediated by miR-376b-3p was counteracted by overexpression of MAP3K1 (Fig. 6E). Consistent with the above findings, MAP3K1 overexpression offset the inhibitory influence of miR-376b-3p on MLE-12 cell apoptosis (Fig. 6F). In addition, MAP3K1 offset the miR-376b-3p-induced reduction in Bax protein levels and elevation of Bcl-2 levels as shown by western blotting (Fig. 6G), which further verified that miR-376b-3p hampers MLE-12 cell apoptosis. Hence, it can be concluded that miR-376b-3p overexpression attenuates LPS-induced MLE-12 cell injury and inflammation by downregulating MAP3K1.

MAP3K1 enhancement reverses the impact of circPalm2 knockdown on LPS-induced MLE-12 cell apoptosis and inflammation

To investigate whether silencing circPalm2 affects LPS-triggered MLE-12 cell damage and inflammation by regulating MAP3K1 expression in ALI, rescue experiments were conducted. CircPalm2 depletion enhanced LPS-stimulated MLE-12 cell viability, while MAP3K1 overexpression counteracted the promoting effect, as demonstrated by CCK-8 assays (Fig. 7A). ELISA showed that MAP3K1 upregulation reversed the suppression of the concentration of proinflammatory factors induced by silencing circPalm2 in LPS-stimulated MLE-12 cells (Fig. 7B). According to flow cytometry analysis, G1-S cell cycle transition was facilitated by circPalm2 depletion, and the promoting effect was reversed by upregulated MAP3K1 (Fig. 7C). In addition, LPS-enhanced MLE-12 cell apoptosis was inhibited by sh-circPalm2, and this inhibition was offset by MAP3K1 overexpression (Fig. 7D, E). Western blotting showed that the reduction in Bax protein expression and the increase in Bcl-2 protein expression caused by circPalm2 silencing were neutralized by MAP3K1 elevation in LPS-stimulated MLE-12 cells (Fig. 7F). Taken together, MAP3K1 upregulation breaks through the restriction that circPalm2 downregulation exerts on LPS-evoked MLE-12 cell apoptosis, cell cycle progression, and inflammatory response.

The expression of circPalm2, miR-376b-3p and MAP3K1 in the lung tissues of CLP-induced ALI mice

To examine the levels of circPalm2, miR-376b-3p and MAP3K1 and their regulatory relationship in septic ALI in vivo, animal models were established utilizing C57BL/6 mice subjected to CLP. As Fig. 8A–C shows, CLP-treated mice exhibited low miR-376b-3p expression and high levels of circPalm2 and MAP3K1 in their lung tissues. In addition, injection of Ad-Sh-circPalm2 contributed to increased miR-376b-3p levels and decreased levels of circPalm2 and MAP3K1 in the lung tissue of the CLP + Ad-Sh-circPalm2 group in comparison to those in the CLP + Ad-NC group (Fig. 8A–C). In addition, a negative correlation between miR-376b-3p and circPalm2 was observed in the lung tissues of CLP-injected mice (n = 24), as presented by Pearson correlation analysis (Fig. 8D). The MAP3K1 level was inversely correlated with the miR-376b-3p level and was positively associated with circPalm2 expression in the lung tissues of mice after CLP surgery (n = 24) (Fig. 8E, F).

Since the circPalm2/miR-330-5p/ROCK2 axis has previously been reported to be involved in ALI [38], miR-330-3p and ROCK2 expression, as well as their expression correlations, were also analysed in lung tissues. As shown by Fig. 8G and H, CLP induced low miR-330-5p levels and high ROCK2 expression in vivo compared to the sham-operated group, and Ad-Sh-circPalm2 induced increased miR-330-5p levels and reduced ROCK2 expression in lung tissue. Moreover, a negative expression correlation between miR-330-5p and ROCK2 and between circPalm2 and miR-330-5p was identified in lung tissue (Fig. 8I, J). Additionally, circPalm2 levels were positively correlated with ROCK2 levels in vivo (Fig. 8K). Collectively, circPalm2 negatively regulates the pulmonary level of miR-376b-3p but positively modulates MAP3K1 pulmonary expression in CLP-induced ALI mice.

Knockdown of circPalm2 inhibits lung injury in CLP-induced ALI mice

In this section, we further probed the effect of circPalm2 silencing in CLP-induced ALI mice. As shown by H&E staining, morphologically normal alveoli were seen in the sham group (Fig. 9A). In comparison to the sham-operated mice, CLP-treated mice showed obvious pathological alterations in their lung tissues, as evidenced by thickened alveolar septa and walls, vascular bleeding, congestion, and collapsed alveolar sacs (Fig. 9A). In contrast, these histologic alterations induced by CLP surgery were mitigated by injection with Ad-Sh-circPalm2 (Fig. 9A). As Fig. 9B illustrates, the CLP group had a much higher injury score than the sham-operated group, while the CLP + Ad-Sh-circPalm2
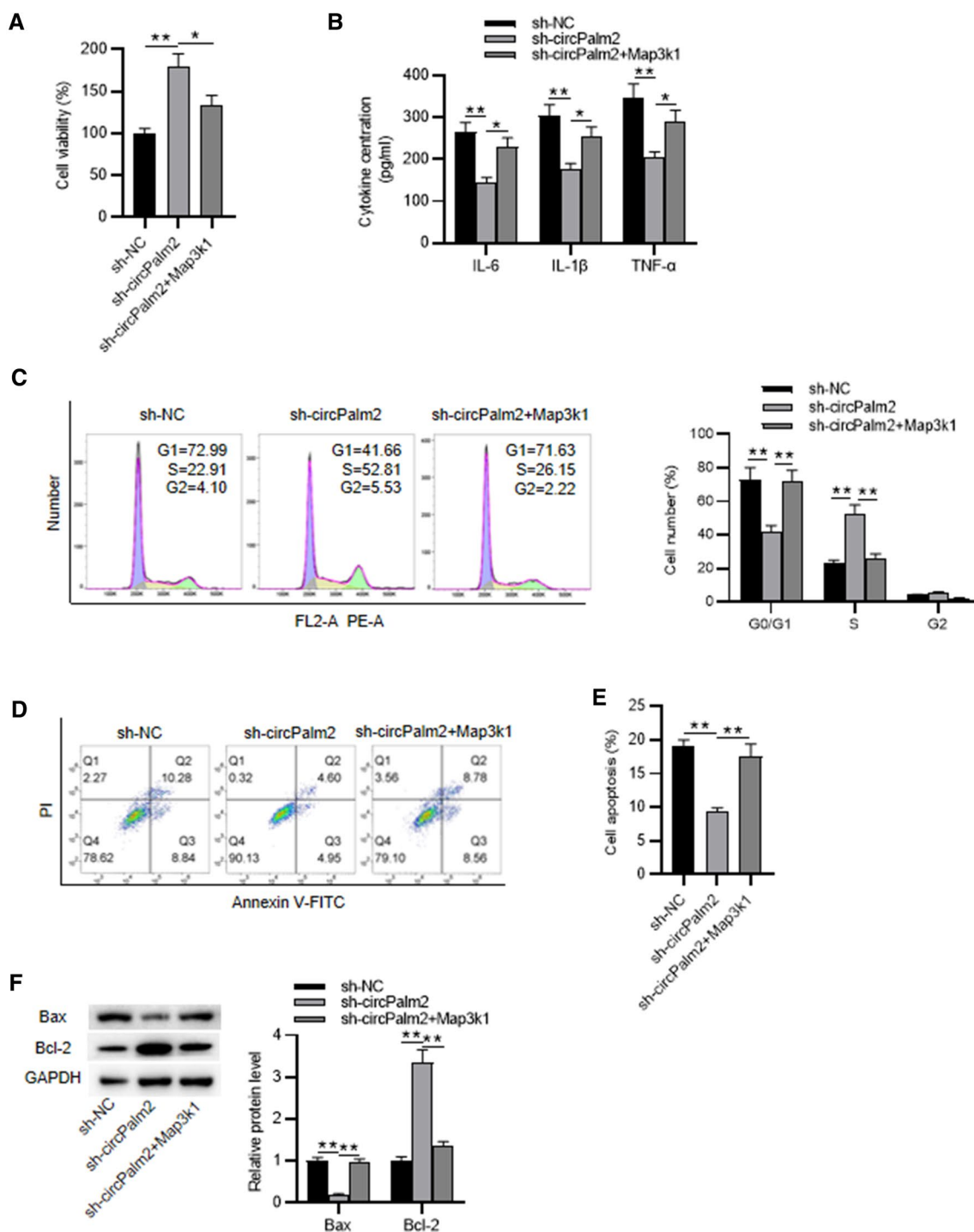
Fig. 7 MAP3K1 enhancement reverses the impact of circPalm2 knockdown on LPS-induced MLE-12 cell apoptosis and inflammation. (**A**) CCK-8 assay for evaluating LPS-treated MLE-12 cell viability after downregulation of circPalm2 alone or simultaneous downregulation of circPalm2 and overexpression of MAP3K1. (**B**) ELISA for determining the proinflammatory cytokine concentrations in LPS-stimulated MLE-12 cells after downregulation of circPalm2 alone or simultaneous downregulation of circPalm2 and overexpression of MAP3K1. (**C–E**) Flow cytometry analysis for determining LPS-treated MLE-12 cell cycle transition and apoptosis after downregulation of circPalm2 alone or simultaneous downregulation of circPalm2 and overexpression of MAP3K1. (**F**) Western blotting for determining apoptosis-related marker protein levels in LPS-stimulated MLE-12 cells after downregulation of circPalm2 alone or simultaneous downregulation of circPalm2 and overexpression of MAP3K1. $*p < 0.05$, $**p < 0.01$
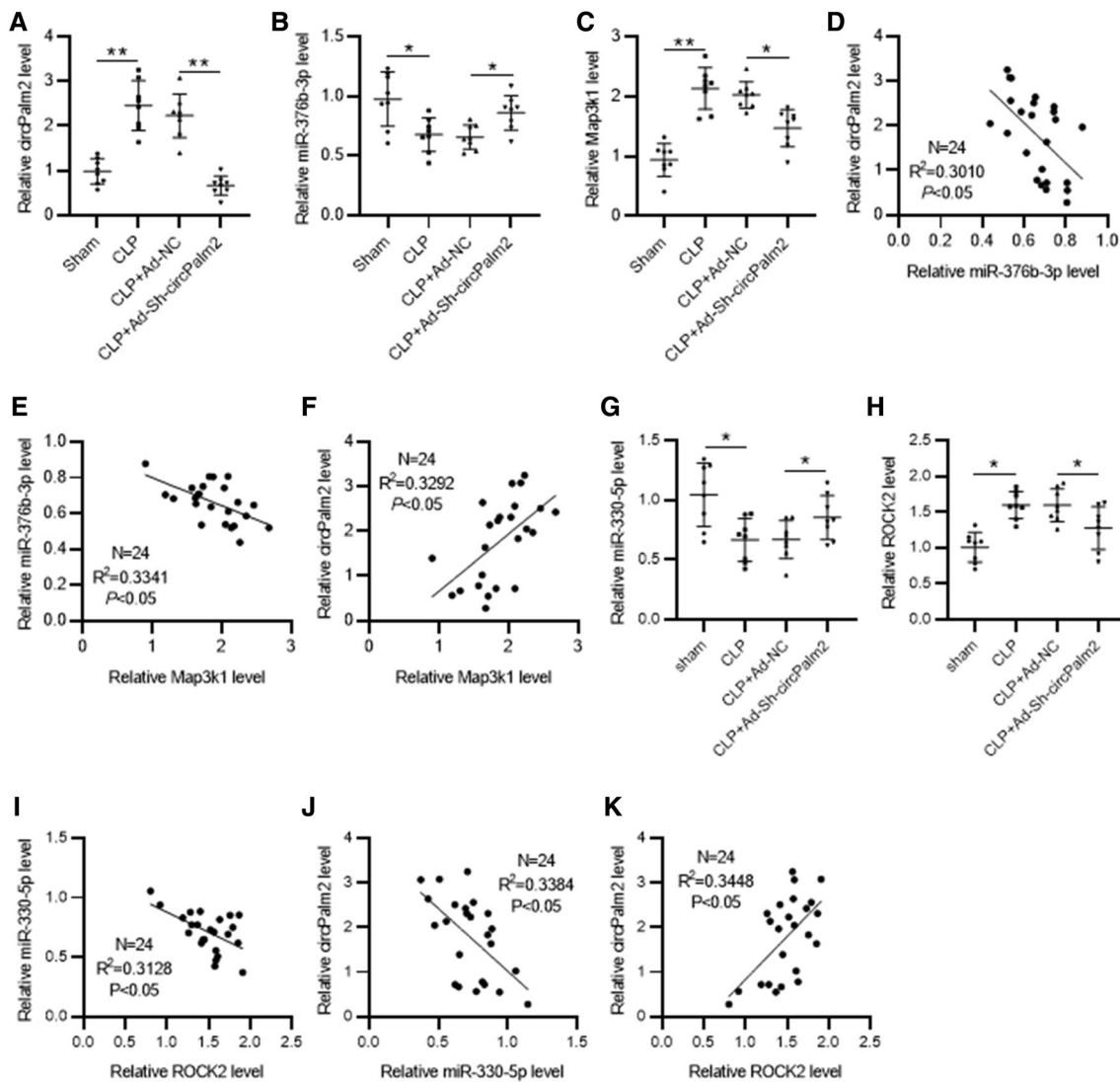
Fig. 8 The expression of circPalm2, miR-376b-3p and MAP3K1 in the lung tissues of CLP-induced ALI mice. (**A**–**C**) RT−qPCR for evaluating circPalm2, miR-376b-3p and MAP3K1 levels in murine lung tissues from the sham, CLP, CLP+Ad-NC and CLP+Ad-Sh-circPalm2 groups. (**D**–**F**) Pearson correlation analysis of the correlations among circPalm2 expression, miR-376b-3p expression and MAP3K1 expression in the lung tissues of CLP-induced ALI mice (n=24). (**G**, **H**) miR-330-5p and ROCK2 expression levels in lung tissues collected from the four experimental groups were detected by PCR. (**I**–**K**) Expression associations among circPalm2, miR-330-5p, and ROCK2 in lung tissues of CLP-treated ALI mice (n=24) by Pearson correlation analyses. *$p < 0.05$, **$p < 0.01$

group presented a greatly reduced injury score than the CLP+Ad-NC group (Fig. 9B). All of these results suggested that circPalm2 depletion mitigates lung injury in CLP-treated mice. Moreover, a reduction in body weight was noted in mice subjected to CLP surgery relative to the sham-operated mice (Fig. 9C). In contrast, the CLP-induced decrease in body weight was partially offset by injecting Ad-Sh-circPalm2 vectors (Fig. 9C).

Lung inflammation is an important hallmark of ALI [39]. As expected, the CLP group exhibited a higher accumulation of proinflammatory cytokines compared with the sham group (Fig. 9D–F). However, this enhancement of proinflammatory factor secretion in lung tissues of the CLP group was weakened by injection with circPalm2-downregulating adenoviral vectors (Fig. 9D–F). Moreover, after CLP surgery, Bax protein expression was increased, while Bcl-2 protein expression was reduced, and the changes were counteracted by circPalm2 depletion in vivo (Fig. 9G). Overall, downregulation of circPalm2 alleviates LPS-induced pulmonary inflammation and histopathological lesions in mice.
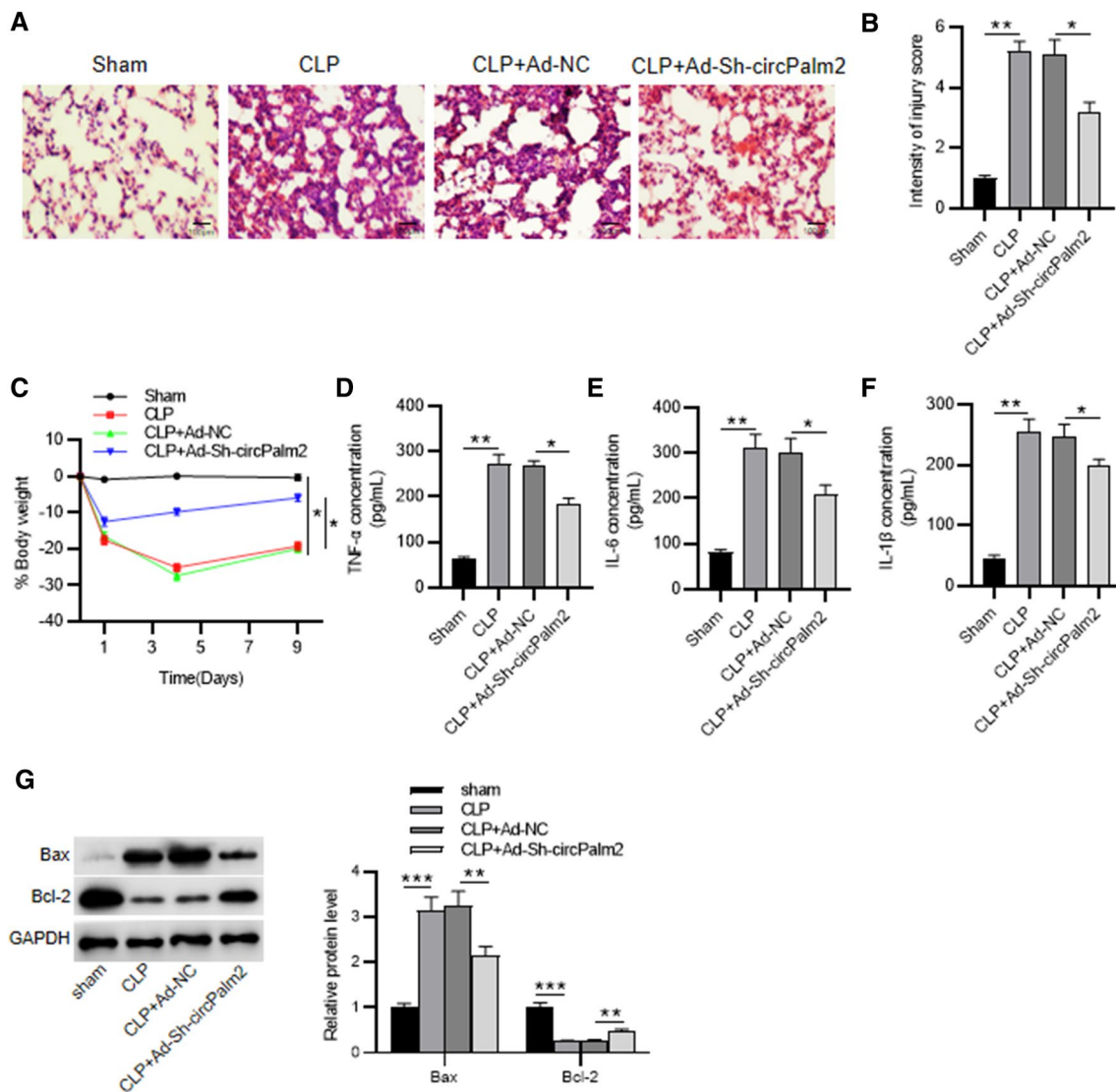
Fig. 9 Knockdown of circPalm2 inhibits lung injury in CLP-treated mice. (**A**) H&E staining to observe the histopathological characteristics of lung tissues from the sham, CLP, CLP + Ad-NC and CLP + Ad-Sh-circPalm2 groups (scale bar = 50 μm). (**B**) Intensity of the injury score of each group. (**C**) Body weight of each group. (**D**–**F**) ELISA for determining the proinflammatory cytokine secretion in each group. (**G**) Western blotting was performed to evaluate the protein levels of apoptosis-related genes (Bax and Bcl-2) in the lung tissue of the four experimental groups. *$p < 0.05$, **$p < 0.01$, ***$p < 0.001$

Silencing circPalm2 inhibits JNK1/2 signalling by downregulating MAP3K1 via miR-376b-3p

The downstream signalling that can be mediated by MAP3K1 was then studied. According to previous reports, MAP3K1 can activate JNK signalling to affect cell apoptosis or survival in many diseases [40–42], and activation of JNK signalling is responsible for ALI aggravation [43, 44]. We found that the phosphorylated JNK1/2 (p-JNK1/2) level was elevated in MLE-12 cells after LPS treatment and that MAP3K1 enhanced the p-JNK1/2 level in LPS-stimulated cells (Fig. 10A). Moreover, overexpressed

miR-376b-3p or silenced circPalm2 suppressed the p-JNK1/2 level in LPS-treated cells, and MAP3K1 overexpression offset the suppressive impacts induced by miR-376b-3p or sh-circPalm2 (Fig. 10B, C). Furthermore, MAP3K1 and p-JNK1/2 levels were increased in the lung tissue of CLP model mice, and injection of Ad-Sh-circPalm2 reduced MAP3K1 and p-JNK1/2 levels in CLP-treated mice (Fig. 10D). The above results demonstrated that MAP3K1 activates JNK1/2 signalling and that circPalm2 deficiency inhibits JNK1/2 signalling by downregulating MAP3K1 via increasing miR-376b-3p.
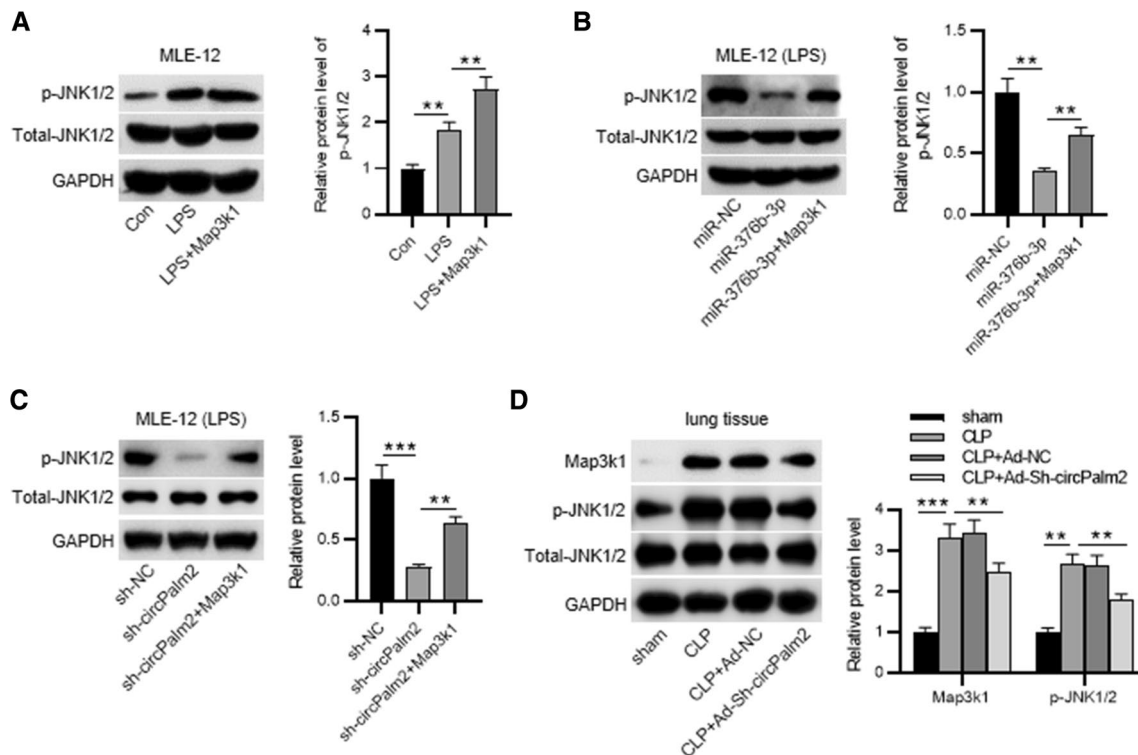
Fig. 10 Silencing circPalm2 inhibits JNK1/2 signalling by downregulating MAP3K1 via miR-376b-3p. Western blotting was performed to quantify phosphorylated JNK1/2 (p-JNK1/2) levels (**A**) in MLE-12 cells of the control group, LPS group, and LPS + MAP3K1 group; (**B**) in LPS-induced MLE-12 cells of the miR-NC, miR-376b-3p, and miR-376b-3p + MAP3K1 groups; (**C**) in LPS-stimulated MLE-12 cells of the sh-NC, sh-circPalm2, and sh-circPalm2 + MAP3K1 groups. (**D**) MAP3K1 and p-JNK1/2 levels in lung tissues of the sham group, CLP group, CLP + Ad-NC, and CLP + Ad-Sh-circPalm2 group were quantitated by western blotting. **$*p < 0.01$, $***p < 0.001$
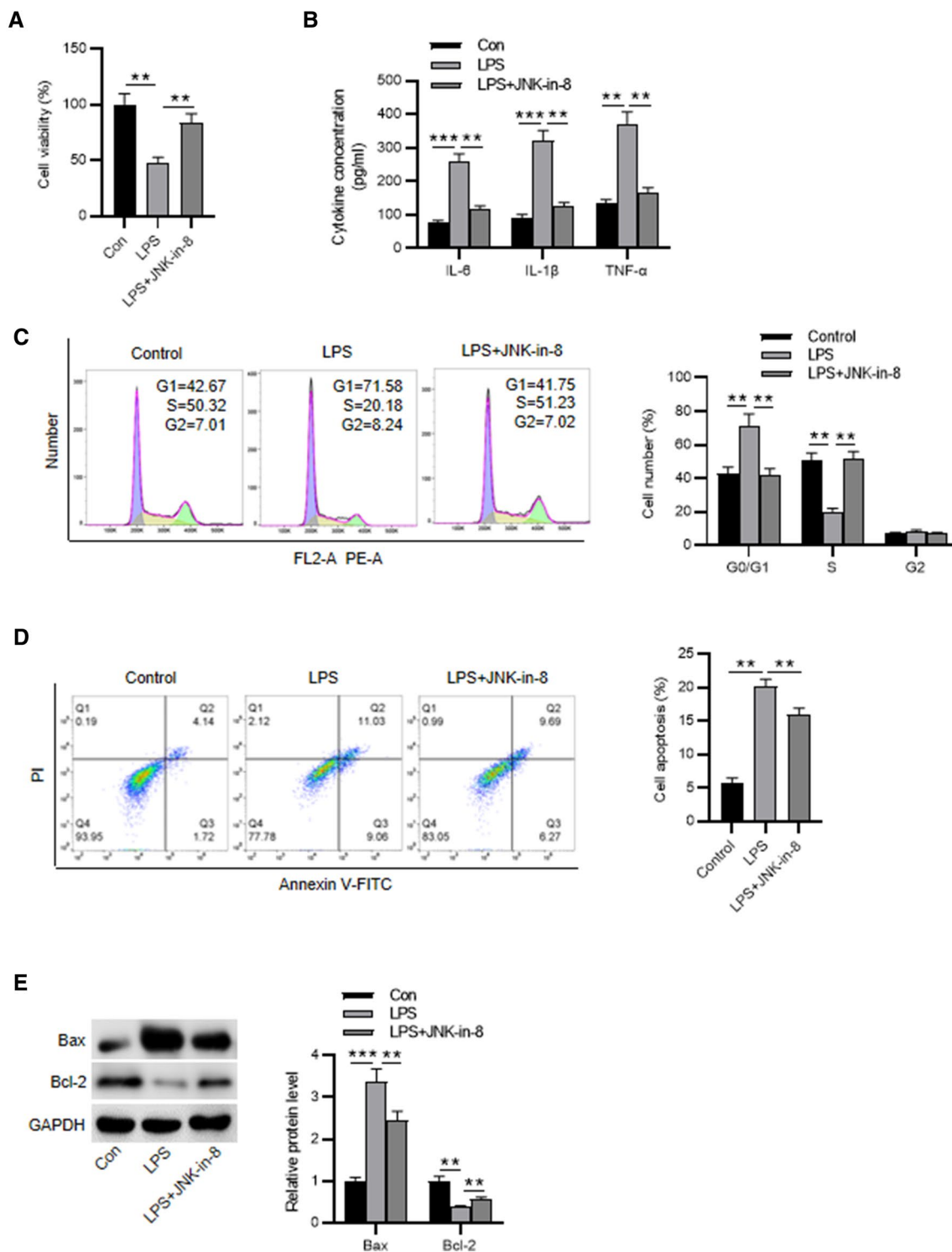
Inhibition of JNK1/2 signalling ameliorates LPS-induced cell injury and inflammation

Finally, we revealed the influence of JNK1/2 signalling on LPS-stimulated MLE-12 cell injury and inflammation. As shown in Fig. 11A, cell viability was greatly reduced after LPS treatment, and the decrease was rescued by JNK-in-8 (a JNK1/2 inhibitor). In addition, JNK-in-8 reversed LPS-induced high concentrations of inflammatory factors, as suggested by ELISA (Fig. 11B). Consistent with these findings, LPS-enhanced cell cycle arrest and cell apoptosis were also inhibited after JNK1/2 inhibition (Fig. 11C, D). Western blotting showed that Bax protein expression was increased while Bcl-2 protein expression was reduced after LPS treatment, and these alterations were counteracted by inhibiting JNK1/2 signalling (Fig. 11E). Overall, inhibition of JNK1/2 signaling can attenuate LPS-induced cell damage and inflammation in vitro.

Discussion

ALI is closely associated with sepsis and is also an important cause of the high mortality of sepsis patients [45]. Thus, the underlying molecular mechanisms of septic ALI should be explored for a better understanding of its development. Accumulating evidence has revealed the dysregulation of circRNAs in septic ALI, possibly implicating circRNAs in the progression of this disease [17]. Thus, more work should be done to reveal the biological functions of circRNAs in septic ALI. In the current study, we elucidated that knockdown of circPalm2 mitigates septic ALI progression by suppressing apoptotic activity, inflammation, and lung injury by regulating the miR-376b-3p/MAP3K1 axis.

In septic ALI, the inflammatory reaction cascade can be caused by the accumulation of inflammatory factors. Inhibition of apoptosis and inflammation of the pulmonary

Fig. 11 Inhibition of JNK1/2 signalling ameliorates LPS-induced cell injury and inflammation. After cells were treated with LPS or JNK-in-8, (**A**) a CCK-8 assay was conducted to detect cell viability; (**B**) ELISA was performed to measure the accumulation of inflammatory factors; (**C**, **D**) flow cytometry was utilized for cell cycle and apoptosis detection; and (**E**) western blotting was performed to quantify the protein levels of the apoptosis-related genes (Bax and Bcl-2). **$p < 0.01$, ***$p < 0.001$

epithelium might ameliorate this disease [46]. LPS is commonly utilized to establish ALI cell models [47]. Consistently, we also used LPS to induce ALI in vitro. After LPS stimulation, we found that MLE-12 cell viability was impaired, and MLE-12 cell apoptosis and inflammation were accelerated, which suggested the successful establishment of in vitro models of septic ALI. Herein, we also successfully established in vivo models of septic ALI by treating C57BL/6 mice with CLP surgery. After CLP surgery, we observed severe morphological changes in murine lung tissues, including the collapse of pulmonary alveoli, haemorrhage, and alveolar thickening. Compared to the sham-operated mice, CLP-treated mice exhibited decreased body weight. In addition, CLP surgery also accelerated cell apoptosis in lung tissue samples and stimulated lung inflammation in mice by increasing their proinflammatory factor levels.

CircPalm2 (circ_0001212), a novel circRNA, has been demonstrated to be upregulated in lung tissues of mice with sepsis [21]. A recent study proposed that circPalm2 interacts with miR-330-5p to upregulate ROCK2 expression and thereby accelerate epithelial cell injury [38]. In the mentioned article, circPalm2 depletion ameliorated the LPS-induced inflammatory response and oxidative stress in MLE-12 cells, and the expression of circPalm2, miR-330-5p, and ROCK2 in LPS-induced ALI mice was consistent with the in vitro experiments [38]. Another study reported that circPalm2 knockdown attenuated LPS-induced apoptosis and the inflammatory response in mouse pulmonary microvascular endothelial cells by reducing ROCK1 expression via miR-129-5p upregulation [48].

Despite these two ceRNA networks mediated by circPalm2, the circPalm2/miR-376b-3p/MAP3K1 axis in ALI has not previously been revealed. In this study, we identified circular characteristics and validated the upregulation of circPalm2 in LPS-stimulated MLE-12 cells and lung tissue from mice subjected to CLP surgery. Similarly, circPalm2 depletion attenuated MLE-12 cell apoptosis, cell cycle arrest, and inflammation triggered by LPS, which was consistent with the findings of previous studies. More importantly, in vivo experiments in our study further revealed that silencing circPalm2 alleviated pulmonary morphological abnormalities and inflammatory injury in ALI mice. In contrast to a previous study that established ALI mouse models by stimulating C57BL/J mice with LPS, the current study established sepsis-induced ALI models using CLP surgery. These results implied that circPalm2 downregulation ameliorates septic ALI pathogenesis in vitro and in vivo.

The ceRNA hypothesis is widely studied because of its unique role in the molecular mechanisms of disease progression [49]. In the ceRNA network mediated by circRNA, a shared miRNA serves as a bridge to help circRNA regulate mRNA [23]. Numerous miRNAs have been demonstrated

to affect septic ALI progression [50–52]. In this report, miR-376b-3p was demonstrated to interact with circPalm2. Emerging reports have substantiated that miR-376b-3p participates in regulating the inflammatory response, especially in periodontitis and diabetes-induced vascular injury [53, 54]. In this study, MLE-12 cells and murine lung tissues displayed low miR-376b-3p expression after LPS stimulation. Furthermore, we confirmed the combination and reverse association between miR-376b-3p and circPalm2.

In our study, transcription factor 4 (MAP3K1) was predicted as a target of miR-376b-3p. MAP3K1 is also known as MEKK 1 and MAPKKK1. In our study, MAP3K1 was highly expressed in MLE-12 cells and murine lung tissue after LPS exposure. Moreover, MAP3K1 was reversely regulated by miR-376b-3p and modulated by circPalm2 in a positive manner in MLE-12 cells. In rescue assays, overexpression of MAP3K1 reversed the suppressive impact of circPalm2 deficiency on apoptosis, cell cycle progression, and inflammation in LPS-treated MLE-12 cells. Notably, the proapoptotic and proinflammatory roles of MAP3K1 have been identified in other inflammatory disorders. For example, genetic variation in MAP3K1 is involved in cell apoptosis and inflammation in acute respiratory distress syndrome [55]. In addition, MAP3K1 regulates *Mycoplasma gallisepticum* (HS strain)-induced inflammation via the MAPK and NF-κB pathways [56]. In summary, MAP3K1 enhances LPS-triggered MLE-12 cell damage, thereby promoting the pathology of septic ALI.

MAP3K1 can evoke the activation of JNK signalling, thereby affecting cell apoptosis or survival in many diseases [40–42]. Moreover, activation of JNK signalling aggravates ALI development [43, 44]. JNK is a member of the mitogen-activated protein kinase (MAPK) family [57]. By being phosphorylated by MAP3Ks, JNK can be activated by proinflammatory factors and stress [58]. Many JNK inhibitors have been demonstrated to be promising therapeutic options for ALI treatment. For example, SP600125 ameliorates sepsis-associated lung injury by suppressing endoplasmic reticulum stress and thus inhibiting apoptosis [59]. JNK-in-8, the first irreversible JNK inhibitor, mitigates LPS-induced AKI by suppressing the JNK/NF-κB signalling-induced inflammatory response and oxidative stress [60].

Consistent with previous findings, the current work revealed that JNK-in-8 attenuates LPS-induced cell apoptosis, cell cycle arrest, and the inflammatory response in vitro. Moreover, MAP3K1 activates JNK1/2 signalling, while miR-376b-3p inhibits the activation of JNK1/2 signaling in LPS-stimulated MLE-12 cells. Silencing circPalm2 inhibits phosphorylated JNK1/2 levels by downregulating MAP3K1 via miR-376b-3p. It can be concluded that circPalm2 interacts with miR-376b-3p to upregulate MAP3K1 levels and thus activates JNK1/2 signaling, thereby promoting MLE-12 cell apoptosis, cell cycle arrest, and the inflammatory

response. In other words, silencing circPalm2 represses LPS-induced MLE-12 cell dysfunction and ameliorates lung injury in CLP-treated mice via regulation of the miR-376b-3p/MAP3K1/JNK1/2 pathway.

The findings of this study might provide novel biomarkers for improving the prognosis of patients diagnosed with septic ALI. Additional studies focusing on other molecules involved in the circPalm2/miR-376b-3p/MAP3K1/JNK1/2 pathway and the axes involved in other activities in ALI, such as oxidative stress, are needed.

Declarations

Conflict of interest The authors declare no conflicts of interest.

Ethical approval This article does not contain any studies with human participants performed by any of the authors.

References

1. Uhle F, Lichtenstern C, Brenner T, Weigand MA (2015) [Pathophysiology of sepsis]. Anasthesiol Intensivmed Notfallmed Schmerzther 50:114–122. https://doi.org/10.1055/s-0041-100391
2. Napolitano LM (2018) Sepsis 2018: definitions and guideline changes. Surg Infect (Larchmt) 19:117–125. https://doi.org/10.1089/sur.2017.278
3. Aziz M, Ode Y, Zhou M, Ochani M, Holodick NE, Rothstein TL, Wang P (2018) B-1a cells protect mice from sepsis-induced acute lung injury. Mol Med 24:26. https://doi.org/10.1186/s10020-018-0029-2
4. Li R, Ren T, Zeng J (2019) Mitochondrial coenzyme Q protects sepsis-induced acute lung injury by activating PI3K/Akt/GSK-3β/mTOR pathway in rats. Biomed Res Int 2019:5240898. https://doi.org/10.1155/2019/5240898
5. Park I, Kim M, Choe K, Song E, Seo H, Hwang Y, Ahn J, Lee SH, Lee JH, Jo YH, Kim K, Koh GY, Kim P (2019) Neutrophils disturb pulmonary microcirculation in sepsis-induced acute lung injury. Eur Respir J 53:1800786. https://doi.org/10.1183/13993003.00786-2018
6. Ling L, Tong J, Zeng L (2020) [Paeoniflorin improves Acute Lung Injury in Sepsis by activating Nrf2/Keap1 signaling pathway]. Sichuan Da Xue Xue Bao Yi Xue Ban 51:664–669. https://doi.org/10.12182/20200960201
7. Xu Q, Wang J (2020) IGFBP7 aggravates sepsis-induced acute lung injury by activating the ERK1/2 pathway. Folia Histochem Cytobiol 58:247–254. https://doi.org/10.5603/FHC.a2020.0028
8. Martin TR, Nakamura M, Matute-Bello G (2003) The role of apoptosis in acute lung injury. Crit Care Med 31:S184–S188. https://doi.org/10.1097/01.Ccm.0000057841.33876.B1
9. Parsons PE, Eisner MD, Thompson BT, Matthay MA, Ancukiewicz M, Bernard GR, Wheeler AP (2005) Lower tidal volume ventilation and plasma cytokine markers of inflammation in patients with acute lung injury. Crit Care Med 33:1–6. https://doi.org/10.1097/01.ccm.0000149854.61192.dc
10. Meduri GU, Kohler G, Headley S, Tolley E, Stentz F, Postlethwaite A (1995) Inflammatory cytokines in the BAL of patients with ARDS. Persistent elevation over time predicts poor outcome. Chest 108:1303–1314. https://doi.org/10.1378/chest.108.5.1303
11. Patop IL, Wüst S, Kadener S (2019) Past, present, and future of circRNAs. EMBO J 38:e100836. https://doi.org/10.15252/embj.2018100836
12. Yu T, Wang Y, Fan Y, Fang N, Wang T, Xu T, Shu Y (2019) CircRNAs in cancer metabolism: a review. J Hematol Oncol 12:90. https://doi.org/10.1186/s13045-019-0776-8
13. Altesha MA, Ni T, Khan A, Liu K, Zheng X (2019) Circular RNA in cardiovascular disease. J Cell Physiol 234:5588–5600. https://doi.org/10.1002/jcp.27384
14. Cao Q, Guo Z, Du S, Ling H, Song C (2020) Circular RNAs in the pathogenesis of atherosclerosis. Life Sci 255:117837. https://doi.org/10.1016/j.lfs.2020.117837
15. Beltrán-García J, Osca-Verdegal R, Nacher-Sendra E, Pallardó FV, García-Giménez JL (2020) Circular RNAs in sepsis: biogenesis, function, and clinical significance. Cells 9:1544. https://doi.org/10.3390/cells9061544
16. Zang J, Lu D, Xu A (2020) The interaction of circRNAs and RNA binding proteins: an important part of circRNA maintenance and function. J Neurosci Res 98:87–97. https://doi.org/10.1002/jnr.24356
17. Yuan C, Gu J, Wu J, Yin J, Zhang M, Miao H, Li J (2020) Circular RNA expression in the lungs of a mouse model of sepsis induced by cecal ligation and puncture. Heliyon 6:e04532. https://doi.org/10.1016/j.heliyon.2020.e04532
18. Yang CL, Yang WK, He ZH, Guo JH, Yang XG, Li HB (2021) Quietness of circular RNA circ_0054633 alleviates the inflammation and proliferation in lipopolysaccharides-induced acute lung injury model through NF-κB signaling pathway. Gene 766:145153. https://doi.org/10.1016/j.gene.2020.145153
19. Bao X, Zhang Q, Liu N, Zhuang S, Li Z, Meng Q, Sun H, Bai J, Zhou X, Tang L (2019) Characteristics of circular RNA expression of pulmonary macrophages in mice with sepsis-induced acute lung injury. J Cell Mol Med 23:7111–7115. https://doi.org/10.1111/jcmm.14577
20. Ma K, Wang W, Gao C, He J (2021) The role of circTMOD3 in regulating LPS-induced acute inflammation and injury in human lung fibroblast WI-38 cells. Exp Lung Res 47:311–322. https://doi.org/10.1080/01902148.2021.1940376
21. Zou Z, Wang Q, Zhou M, Li W, Zheng Y, Li F, Zheng S, He Z (2020) Protective effects of P2X7R antagonist in sepsis-induced acute lung injury in mice via regulation of circ_0001679 and circ_0001212 and downstream pln, Cdh2, and Nprl3 expression. J Gene Med 22:e3261. https://doi.org/10.1002/jgm.3261
22. Chen LL (2020) The expanding regulatory mechanisms and cellular functions of circular RNAs. Nat Rev Mol Cell Biol 21:475–490. https://doi.org/10.1038/s41580-020-0243-y
23. Zhu J, Zhang X, Gao W, Hu H, Wang X, Hao D (2019) lncRNA/circRNA–miRNA–mRNA ceRNA network in lumbar intervertebral disc degeneration. Mol Med Rep 20:3160–3174. https://doi.org/10.3892/mmr.2019.10569
24. Correia de Sousa M, Gjorgjieva M, Dolicka D, Sobolewski C, Foti M (2019) Deciphering miRNAs' action through miRNA editing. Int J Mol Sci 20:6249. https://doi.org/10.3390/ijms20246249

25. Jiang WY, Ren J, Zhang XH, Lu ZL, Feng HJ, Yao XL, Li DH, Xiong R, Fan T, Geng Q (2020) CircC3P1 attenuated pro-inflammatory cytokine production and cell apoptosis in acute lung injury induced by sepsis through modulating miR-21. J Cell Mol Med 24:11221–11229. https://doi.org/10.1111/jcmm.15685

26. Zhao D, Wang C, Liu X, Liu N, Zhuang S, Zhang Q, Bao X, Xu S, Zhou X, Meng Q, Li S, Tang L (2021) CircN4bp1 facilitates sepsis-induced acute respiratory distress syndrome through mediating macrophage polarization via the miR-138-5p/EZH2 axis. Mediators Inflamm 2021:7858746. https://doi.org/10.1155/2021/7858746

27. Lin Q, Liang Q, Qin C, Li Y (2021) CircANKRD36 Knockdown suppressed cell viability and migration of LPS-stimulated RAW264.7 cells by sponging MiR-330. Inflammation 44:2044–2053. https://doi.org/10.1007/s10753-021-01480-5

28. Ji Q, Sun Z, Yang Z, Zhang W, Ren Y, Chen W, Yao M, Nie S (2021) Protective effect of ginsenoside Rg1 on LPS-induced apoptosis of lung epithelial cells. Mol Immunol 136:168–174. https://doi.org/10.1016/j.molimm.2018.11.003

29. Lipner MB, Peng XL, Jin C, Xu Y, Gao Y, East MP, Rashid NU, Moffitt RA, Herrera Loeza SG, Morrison AB, Golitz BT, Vaziri C, Graves LM, Johnson GL, Yeh JJ (2020) Irreversible JNK1-JUN inhibition by JNK-IN-8 sensitizes pancreatic cancer to 5-FU/FOLFOX chemotherapy. JCI Insight 5:2. https://doi.org/10.1172/jci.insight.129905

30. Sun H, Hu H, Xu X, Fang M, Tao T, Liang Z (2021) Protective effect of dexmedetomidine in cecal ligation perforation-induced acute lung injury through HMGB1/RAGE pathway regulation and pyroptosis activation. Bioengineered 12:10608–10623. https://doi.org/10.1080/21655979.2021.2000723

31. Zhang J, Zheng Y, Wang Y, Wang J, Sang A, Song X, Li X (2022) YAP1 alleviates sepsis-induced acute lung injury via inhibiting ferritinophagy-mediated ferroptosis. Front Immunol 13:884362. https://doi.org/10.3389/fimmu.2022.884362

32. Qiu N, Xu X, He Y (2020) LncRNA TUG1 alleviates sepsis-induced acute lung injury by targeting miR-34b-5p/GAB1. BMC Pulm Med 20:49. https://doi.org/10.1186/s12890-020-1084-3

33. Matute-Bello G, Downey G, Moore BB, Groshong SD, Matthay MA, Slutsky AS, Kuebler WM (2011) An official american thoracic society workshop report: features and measurements of experimental acute lung injury in animals. Am J Respir Cell Mol Biol 44:725–738. https://doi.org/10.1165/rcmb.2009-0210ST

34. Nagura-Ikeda M, Imai K, Tabata S, Miyoshi K, Murahara N, Mizuno T, Horiuchi M, Kato K, Imoto Y, Iwata M, Mimura S, Ito T, Tamura K, Kato Y (2020) Clinical evaluation of self-collected saliva by quantitative reverse transcription-PCR (RT-qPCR), direct RT-qPCR, reverse transcription-loop-mediated isothermal amplification, and a rapid antigen test to diagnose COVID-19. J Clin Microbiol 58:e01438–20. https://doi.org/10.1128/jcm.01438-20

35. Li JH, Liu S, Zhou H, Qu LH, Yang JH (2014) starBase v2.0: decoding miRNA-ceRNA, miRNA-ncRNA and protein-RNA interaction networks from large-scale CLIP-Seq data. Nucleic Acids Res 42:D92–D97. https://doi.org/10.1093/nar/gkt1248

36. Lewis BP, Burge CB, Bartel DP (2005) Conserved seed pairing, often flanked by adenosines, indicates that thousands of human genes are microRNA targets. Cell 120:15–20. https://doi.org/10.1016/j.cell.2004.12.035

37. Ye Z, Liu X, Yang Y, Zhang X, Yu T, Li S, Feng Y, Luo G (2018) The differential expression of novel circular RNAs in an acute lung injury rat model caused by smoke inhalation. J Physiol Biochem 74:25–33. https://doi.org/10.1007/s13105-017-0598-5

38. Ren Y, Li L, Wang M, Yang Z, Sun Z, Zhang W, Cao L, Nie S (2022) Knockdown of circRNA paralemmin 2 ameliorates lipopolysaccharide-induced murine lung epithelial cell Injury by sponging mir-330-5p to reduce ROCK2 expression. Immunol

Invest 51:1707–1724. https://doi.org/10.1080/08820139.2022.2027961

39. Cheng N, Liang Y, Du X, Ye RD (2018) Serum amyloid A promotes LPS clearance and suppresses LPS-induced inflammation and tissue injury. EMBO Rep 19:e45517. https://doi.org/10.15252/embr.201745517

40. Chang Y, Yan W, Sun C, Liu Q, Wang J, Wang M (2017) Mir-145-5p inhibits epithelial-mesenchymal transition via the JNK signaling pathway by targeting MAP3K1 in non-small cell lung cancer cells. Oncol Lett 14:6923–6928. https://doi.org/10.3892/ol.2017.7092

41. Pham TT, Angus SP, Johnson GL (2013) MAP3K1: genomic alterations in Cancer and function in promoting cell survival or apoptosis. Genes Cancer 4:419–426. https://doi.org/10.1177/1947601913513950

42. Parker A, Cross SH, Jackson IJ, Hardisty-Hughes R, Morse S, Nicholson G, Coghill E, Bowl MR, Brown SD (2015) The goya mouse mutant reveals distinct newly identified roles for MAP3K1 in the development and survival of cochlear sensory hair cells. Dis Model Mech 8:1555–1568. https://doi.org/10.1242/dmm.023176

43. Hui Z, Jie H, Fan GH (2021) Expression of DUSP12 reduces lung vascular endothelial cell damage in a murine model of lipopolysaccharide-induced acute lung injury via the apoptosis signal-regulating kinase 1 (ASK1)-Jun N-Terminal kinase activation (JNK) pathway. Med Sci Monit 27:e930429. https://doi.org/10.12659/msm.930429

44. Wang WB, Li JT, Hui Y, Shi J, Wang XY, Yan SG (2022) Combination of pseudoephedrine and emodin ameliorates LPS-induced acute lung injury by regulating macrophage M1/M2 polarization through the VIP/cAMP/PKA pathway. Chin Med 17:19. https://doi.org/10.1186/s13020-021-00562-8

45. Chen Q, Shao X, He Y, Lu E, Zhu L, Tang W (2021) Norisoboldine attenuates sepsis-induced acute lung injury by modulating macrophage polarization via PKM2/HIF-1α/PGC-1α pathway. Biol Pharm Bull 44:1536–1547. https://doi.org/10.1248/bpb.b21-00457

46. Baradaran Rahimi V, Rakhshandeh H, Raucci F, Buono B, Shirazinia R, Samzadeh Kermani A, Maione F, Mascolo N, Askari VR (2019) Anti-inflammatory and anti-oxidant activity of Portulaca oleracea extract on LPS-induced rat lung injury. Molecules 24:139. https://doi.org/10.3390/molecules24010139

47. Sakhatskyy P, Wang Z, Borgas D, Lomas-Neira J, Chen Y, Ayala A, Rounds S, Lu Q (2017) Double-hit mouse model of cigarette smoke priming for acute lung injury. Am J Physiol Lung Cell Mol Physiol 312:L56. https://doi.org/10.1152/ajplung.00436.2016

48. Mu Q, Zhang C, Li R, Guo Z (2022) CircPalm2 knockdown alleviates LPS-evoked pulmonary microvascular endothelial cell apoptosis and inflammation via miR-450b-5p/ROCK1 axis. Int Immunopharmacol 113:109199. https://doi.org/10.1016/j.intimp.2022.109199

49. Tay Y, Rinn J, Pandolfi PP (2014) The multilayered complexity of ceRNA crosstalk and competition. Nature 505:344–352. https://doi.org/10.1038/nature12986

50. Gao M, Yu T, Liu D, Shi Y, Yang P, Zhang J, Wang J, Liu Y, Zhang X (2021) Sepsis plasma-derived exosomal mir-1-3p induces endothelial cell dysfunction by targeting SERP1. Clin Sci (Lond) 135:347–365. https://doi.org/10.1042/cs20200573

51. Jiao Y, Zhang T, Zhang C, Ji H, Tong X, Xia R, Wang W, Ma Z, Shi X (2021) Exosomal miR-30d-5p of neutrophils induces M1 macrophage polarization and primes macrophage pyroptosis in sepsis-related acute lung injury. Crit Care 25:356. https://doi.org/10.1186/s13054-021-03775-3

52. Lin J, Lin Z, Lin L (2021) MiR-490 alleviates sepsis-induced acute lung injury by targeting MRP4 in new-born mice. Acta Biochim Pol 68:151–158. https://doi.org/10.18388/abp.2020_5397

53. Tomofuji T, Yoneda T, Machida T, Ekuni D, Azuma T, Kataoka K, Maruyama T, Morita M (2016) MicroRNAs as serum biomarkers for periodontitis. J Clin Periodontol 43:418–425. https://doi.org/10.1111/jcpe.12536

54. Yang B, Gao X, Sun Y, Zhao J, Chen J, Gao L, Zhao L, Li Y (2020) Dihydroartemisinin alleviates high glucose-induced vascular smooth muscle cells proliferation and inflammation by depressing the miR-376b-3p/KLF15 pathway. Biochem Biophys Res Commun 530:574–580. https://doi.org/10.1016/j.bbrc.2020.07.095

55. Morrell ED, O'Mahony DS, Glavan BJ, Harju-Baker S, Nguyen C, Gunderson S, Abrahamson A, Radella F 2, Rona G, Black RA, Wurfel MM (2018) Genetic variation in MAP3K1 associates with ventilator-free days in acute respiratory distress syndrome. Am J Respir Cell Mol Biol 58:117–125. https://doi.org/10.1165/rcmb.2017-0030OC

56. Zhao Y, Zou M, Sun Y, Zhang K, Peng X (2019) Gga-miR-21 modulates Mycoplasma gallisepticum (HS strain)-Induced inflammation via targeting MAP3K1 and activating MAPKs and NF-κB pathways. Vet Microbiol 237:108407. https://doi.org/10.1016/j.vetmic.2019.108407

57. Li G, Qi W, Li X, Zhao J, Luo M, Chen J (2021) Recent advances in c-Jun N-Terminal kinase (JNK) inhibitors. Curr Med Chem 28:607–627. https://doi.org/10.2174/0929867327666200210144114

58. Kim EK, Choi EJ (2010) Pathological roles of MAPK signaling pathways in human diseases. Biochim Biophys Acta 1802:396–405. https://doi.org/10.1016/j.bbadis.2009.12.009

59. Lou L, Hu D, Chen S, Wang S, Xu Y, Huang Y, Shi Y, Zhang H (2019) Protective role of JNK inhibitor SP600125 in sepsis-induced acute lung injury. Int J Clin Exp Pathol 12:528–538

60. Du J, Wang G, Luo H, Liu N, Xie J (2021) JNK-IN-8 treatment alleviates lipopolysaccharide-induced acute lung injury via suppression of inflammation and oxidative stress regulated by JNK/NF–κB signaling. Mol Med Rep 23:150. https://doi.org/10.3892/mmr.2020.11789